# HIGH PRECISION GRAVITY MEASUREMENTS USING ATOM INTERFEROMETRY

Achim Peters, Keng Yeow Chung, and Steven Chu
*Physics Department, Stanford University, Stanford, CA 94305-4060, USA*

We present an atom interferometer that has been used to measure $g$, the local acceleration due to gravity, with a resolution of $\Delta g/g = 1 \times 10^{-10}$ and an estimated acuracy of $3 \times 10^{-9}$ $g$. The value of $g$ obtained by this quantum mechanical measurement and the value obtained by dropping an macroscopic object agree with an uncertainty of $7 \times 10^{-9}$, providing the best evidence so far for the validity of the weak equivalence principle at the quantum level.

## 1 Introduction

Since 1991, when the first matter–wave interferometers[1,2,3,4] using neutral atoms were demonstrated, the performance of such atom interferometers has improved substantially. By now, they can be used to perform a variety of measurements with a precision and accuracy that challenges, if not exceeds, that of any competing instrument. Here we demonstrate this for the measurement $g$, the local acceleration due to gravity.

Measuring $g$, a site dependent quantity that also varies with time, is interesting for a variety of reasons, including applications in geophysics and metrology.[5] Precise measurements of $g$ are also useful for locating oil, water and other natural resources. These applications require measurement precisions ranging from $10^{-6}$ to $10^{-9}$ (See Table 1 for the magnitude of some gravitational effects). The Performance parameters of commonly used gravimeters are listed in Table 2. Currently, the best absolute gravimeters are falling corner–cube instruments which can obtain an gravity value accurate to approximately 2 $\mu$Gal.[a] They are a proven reference against which we can compare our interferometer.

To measure $g$, we use an atom interferometer that uses laser cooled atoms in an atomic fountain to achieve long measurement times. The interferometer employs atom optical components based on pulses of light which drive stimulated Raman transitions between stable hyperfine ground states. The main advantages of this two-photon technique are the nearly infinite lifetime of the involved atomic states and a measurement resolution that depends only on the stability of the frequency *difference* of the two laser beams, which can be phase-locked to a stable microwave source, referenced in turn to an atomic clock. This method has already been used to measure photon recoil[10,11] and rotations[12] with very high precision. We used it in 1991 to measure $g$ with a resolution of $3 \times 10^{-8}$ after 40 minutes of integration time.[4]

Stimulated Raman transitions have been discussed elsewhere in great detail.[13,14] The basic process is illustrated in Fig. 1 and can be summarized as follows:

[a] 1 $\mu$Gal = $10^{-6}$ cm/s$^2$ = $10^{-8}$ m/s$^2$ $\approx$ $10^{-9}$ $g$.

| **Spatial gravity variations** | |
|---|---|
| • gravity gradient | $\sim 3 \times 10^{-7}$ g/m |
| • global scale | $\sim 10^{-3}$ g |
| • regional scale (useful for navigation, prospecting, archeology, ...) | $\sim 10^{-6}$ g |
| **Temporal gravity variations** | |
| • tides | $\sim 10^{-7}$ g |
| • man-made environmental changes | $\sim 10^{-9}$ g |
| • atmospheric pressure | $\sim 3 \times 10^{-10}$ g/mbar |
| • local water table | $\sim 10^{-8}$ g |
| • ... | $\sim 10^{-9}$ g |

Table 1: Important gravitational effects and their typical magnitude.

| Type of gravimeter | Noise ($g/\sqrt{Hz}$) | Drift (g/day) | Accuracy (g) |
|---|---|---|---|
| **Spring/mass systems** A very stable, well characterized and temperature controlled spring supports a test mass against gravity. Variations in gravity change the spring's extension. Drift caused mostly by aging of spring. Requires frequent re-calibration. Very compact and transportable.[5] | $< 10^{-9}$ | $3 \times 10^{-8}$ | N/A |
| **Cryogenic gravimeters** A superconducting sphere is levitated in a magnetic field and variations in gravity are counterbalanced using force feedback. Drift caused mostly by changing mass of sphere due to cryopumping. Vibration induced flux-jumps in superconductor cause gravity offsets when instrument is moved. Lowest noise of all gravimeters, limited by environment.[5,6,7] | $< 10^{-12}$ | $2 \times 10^{-10}$ | N/A |
| **Falling corner-cubes** A laser interferometer monitors the motion of a freely falling corner-cube retro-reflector. Uses "super-spring" to eliminate effect of high frequency vibrations. Noise depends strongly on site and drop rate. Maximum drop rate 1 Hz, but usually reduced to 1/15 Hz to limit mechanical wear and prevent vibration induced accuracy degradation.[5,8,9] | $1 \times 10^{-7}$ | — | $2 \times 10^{-9}$ |
| **Atom interferometer** See text. | $3 \times 10^{-8}$ | — | $3 \times 10^{-9}$ |

Table 2: Different types of gravimeters and their typical performance. The noise levels for the falling corner-cube gravimeter and the atom interferometer are for measurements in our laboratory. Under ideal conditions the noise of the falling corner-cube gravimeter can be 10 times lower.

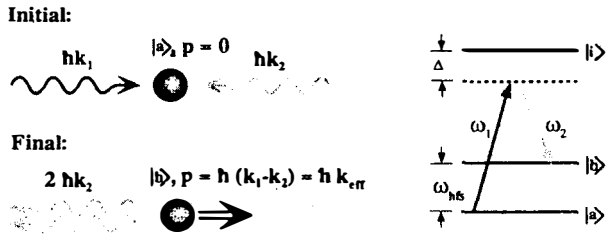


Figure 1: An atom undergoes a stimulated Raman transition. It absorbs a photon of frequency $\omega_1$ and emits another one (via a stimulated emission) of frequency $\omega_2$. Since both photons carry momentum, and because momentum has to be conserved in the process, the atom receives a recoil momentum kick.

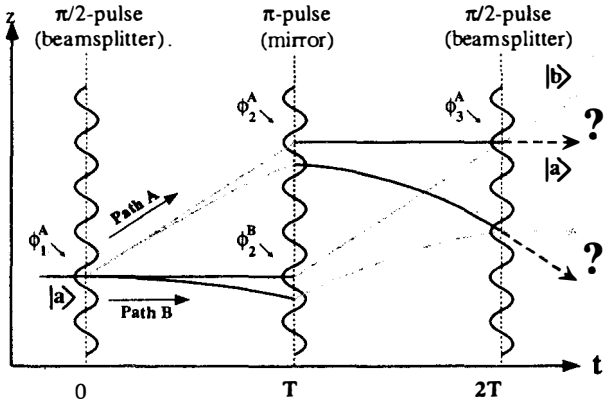


Figure 2: Basic Mach-Zehnder type atom interferometer with (curved lines) and without (straight lines) gravity. The atom can either be in the internal state $|a\rangle$ (dark) or $|b\rangle$ (light). The lines represent the classical trajectories originating from one of the space-time points comprising the initial wave packet.

(a) The atom is illuminated by two counter-propagating laser beams whose frequency difference equals the splitting between two hyperfine ground states of the atom. For this pair of beams we define an effective wave number $\mathbf{k}_{\rm eff} = \mathbf{k}_1 - \mathbf{k}_2$ ($k_{\rm eff} = |\mathbf{k}_2| + |\mathbf{k}_1|$ for counter propagating beams) and an effective frequency $\omega_{\rm eff} = \omega_1 - \omega_2$, where $\mathbf{k}_i$ and $\omega_i$ are the equivalent quantities for the individual laser beams.

(b) Absorption and stimulated emission of photons during a Raman pulse can change the momentum of the atom by $\hbar\mathbf{k}_{\rm eff}$ and, simultaneously, its internal state. The transition probability depends on the pulse area and can be adjusted to create either beam splitters or mirrors.

(c) The quantum mechanical phase of the resulting superposition state depends on the local Raman phase $\phi_i = k_{\rm eff} z_i - \omega_{\rm eff} t_i$.

Figure 2 shows how a sequence of three such Raman pulses is used to split, reflect and recombine an atom while simultaneously changing its internal state. At the end of this sequence the fraction of the atoms in one of the states is detected. The result is an oscillatory function of the interferometer path difference, which, among other things, depends on the gravitational acceleration.

The total phase difference between paths A and B can be divided into two parts. The first

contribution describes the periods of free evolution between laser pulses and is given by

$$\Delta\phi_{\text{path}} = \frac{1}{\hbar}\left(S_{\text{cl}}^{B} - S_{\text{cl}}^{A}\right) \tag{1}$$

in the limit where the classical action

$$S_{\text{cl}} = \int_{0}^{2T} \mathcal{L}\left[z(t), \dot{z}(t)\right] dt \tag{2}$$

along each path is much greater than $\hbar$.[15] For uniform gravitational fields ($\mathcal{L} = \frac{m}{2}v^2 - mgz$) this contribution vanishes.

The second contribution is due to the interaction with the Raman beams. Whenever the state of the atom changes during such an interaction, it acquires an additional phase $\phi_i = k_{\text{eff}} z_i - \omega_{\text{eff}} t_i$, where $z_i$ is the position of the atom at time $t_i$. The sign of the phase depends on the initial state of the atom. Tracing all the state changes we find a phase difference of

$$\Delta\phi_{\text{light}} = (\phi_1^A - \phi_2^A) - (\phi_2^B - \phi_3^A)\,. \tag{3}$$

Without a gravitational field the trajectories are straight lines and the inherent symmetry of the situation (Fig. 2) leads to $\Delta\phi = 0$. The introduction of a gravitational field breaks the symmetry. The atom now falls three times as far during the second half of the interferometer as during the first half and we find a phase shift proportional to the gravitational acceleration:

$$\Delta\phi = k_{\text{eff}} g T^2\,. \tag{4}$$

This simple equation describes the interferometer extremely well and has to be modified only slightly to account for gravity gradients and finite length Raman pulses.[16] The equation also indicates that it is highly desirable to make the time $T$ between the interferometer pulses as long as possible since the measurement sensitivity scales quadratically with $T$. Following our first gravity measurements in 1991 we have thus focused on extending the resolution of the device by increasing the interferometer measurement time by implementing an active vibration isolation system, and by increasing the measurement accuracy by studying and eliminating potential systematic effects.

## 2 Experimental Setup

The experimental setup is shown in Fig. 3. About $\sim 5 \times 10^8$ cesium atoms are extracted from a low pressure background vapor and loaded into a magneto-optic trap[17,18] in 600 ms, forming a $\sim 5$ mm diameter cloud. After turning off the magnetic fields, the atoms are launched vertically using moving optical molasses.[19] During this time the atoms are further cooled by tuning the molasses beams 60 MHz below resonance and lowering the intensity to $5\,\text{mW/cm}^2$. In the final stages of the launch, laser intensities are ramped down in $400\,\mu$s so that the atoms are also adiabatically cooled.[20] The final temperature of the launched atoms is $\sim 1.5\,\mu$K. Their velocity of $\sim 3.0$ m/s places them on trajectories that will peak $\sim 46$ cm above the trap.

After launch, the atoms are subjected to a sequence of microwave, velocity selective Raman, and state selective blow-away pulses that places $3 \times 10^6$ atoms in the $6S_{1/2}$, $F = 3$, $m_F = 0$ state with an effective vertical temperature of $\sim 10$ nK. This low velocity spread gives us a fringe contrast of 65% for all times $T$ between 0.5 ms and 160 ms.

The interferometer measurement occurs in a magnetically shielded region where the atoms are illuminated by a sequence of laser pulses generated by two external-cavity phase-locked diode lasers. The Raman difference frequency is controlled by a direct digital frequency synthesizer which is referenced to a Loran-C frequency standard. The frequency difference is switched

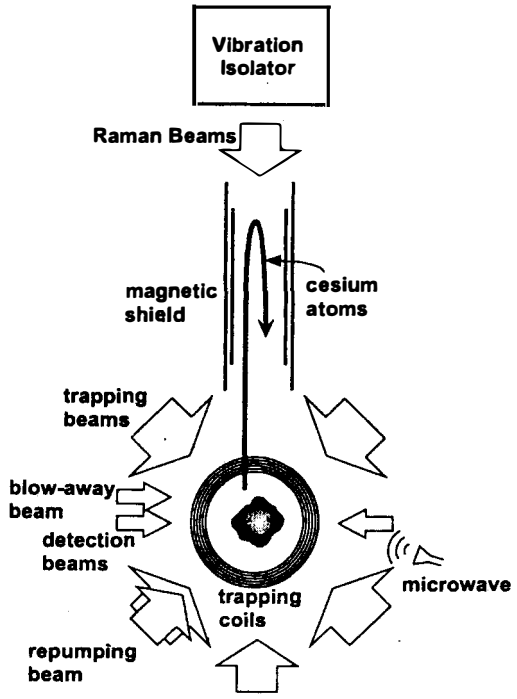


Figure 3: Overview of experimental setup.

between 3 fixed frequencies to compensate for the $\sim$ 7 MHz of gravity-induced Doppler shift during the 320 ms interferometer free-fall time.[16]

As shown in Fig. 3, both Raman beams enter the vacuum chamber from below and are retro-reflected. Since the atomic transitions are Doppler sensitive, only one beam from each pair of upward and downward travelling beams is in resonance with the atoms. Since the two Raman beams travel over a common path before entering the vacuum system, laboratory vibrations frequency shift the two beams by nearly the same amount. Thus, only vibrations of the retro-mirror affect the Raman difference frequency. This mirror is mounted on an actively stabilized, vibration isolation system. The platform has an effective resonance of 0.02 Hz and reduces vibrations between 0.2 Hz to 5 Hz by two orders of magnitude.[21] Without this vibration isolation, our interference fringes vanish for $T > 40$ ms. With the feedback circuit on, there is essentially no loss of fringe contrast up to the maximum drop times, limited by the size of the magnetically shielded region. Further motion control in our apparatus includes an active tilt control to maintain the horizontal position of the retro-mirror to within 10 $\mu$rad, and an additional active system acting on the optical table to reduce table rotations.

The interferometer phase shift, which manifests itself as a modulation of the fraction of atoms in the $F = 4$, $m_F = 0$ state, is finally determined using normalized fluorescence detection. The duration of the complete measurement cycle is 1.3 s.

## 3 Experimental Results

Typical interferometer data for a pulse spacing of $T = 160$ ms is shown in Fig. 4. One minute of integration time allows us to determine g with a precision of $3 \times 10^{-9}\, g$. To locate the central fringe, we vary $T$ from 2 ms to 160 ms. Our uncertainty in determining the center of this fringe

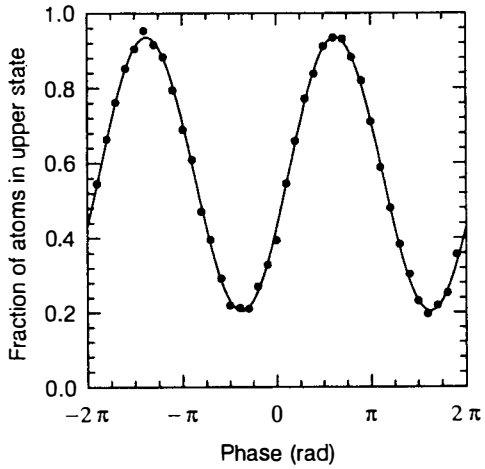


Figure 4: Typical Doppler sensitive interferometer fringe for $T = 160$ ms. Each of the 40 data points represents a single launch of the atoms, spaced 1.3 seconds apart and taken over a period of 1 minute. One full fringe period corresponds to $\sim 2 \times 10^{-6}$ g. Performing a least squares fit determines local gravity to approximately $3 \times 10^{-9}$ g.

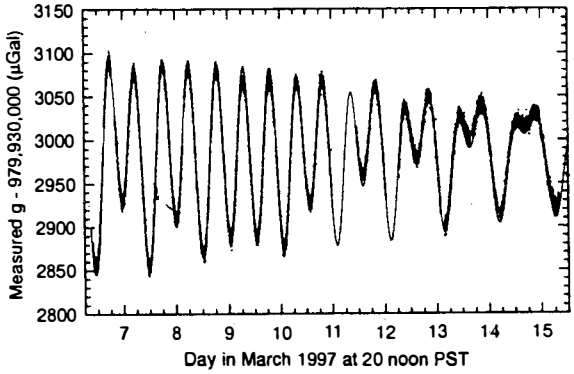


Figure 5: Gravity data taken over a period of 9 days. The data points are spaced approximately 1 minute apart and each corresponds to one of the interferometer fringes shown in Fig. 4. The solid line is a single parameter (vertical offset) fit using a theoretical model of the gravity tides at our measurement site (Stanford, California).

results in $\delta g/g \sim 3 \times 10^{-9}$.

Figure 5 shows a continuous measurement of $g$ over a period of 9 days, with each dot corresponding to data similar to Fig. 4. The complicated time dependence is due to tidal forces and can in principle be predicted by appropriate theoretical models. To achieve our targeted measurement accuracy, however, these models have to be quite sophisticated and include deformations of the local tectonic plate due to ocean loading effects.[22,23] The solid line in Fig. 5 is a single parameter fit (vertical offset) using one such model.[24,25]

During the course of our experiment we have arranged for an Micro-g Solutions FG5 absolute gravimeter[9] to be run in our laboratory for three days to measure the absolute value of $g$. This is a Michelson optical interferometer with one arm defined by a freely falling corner-cube and has a quoted uncertainty of 2 ppb.

The data from the comparison measurement is summarized in Fig. 6. It shows that our atom interferometer has 3 times higher resolution than the falling corner cube gravimeter, mainly due to slower FG-5 repetition rate (1/15 Hz) compared with our instrument (1/1.3 Hz). The noise per launch for both instruments was similar.

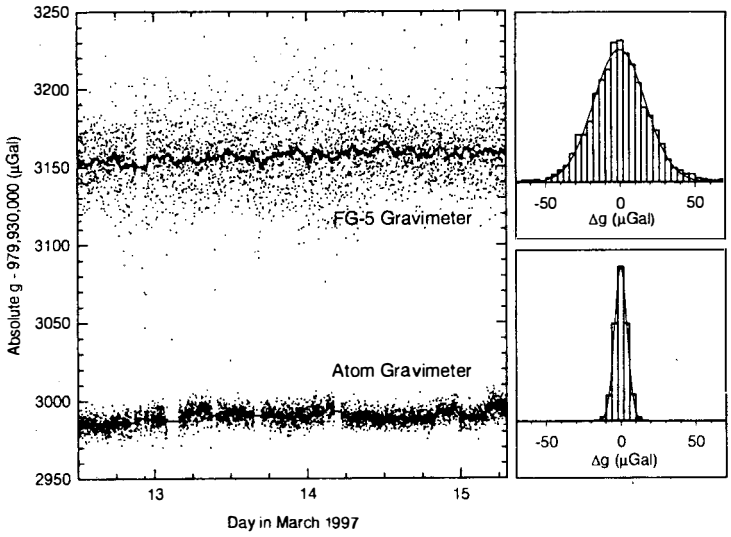


Figure 6: Comparison between atom interferometer (lower dataset) and classical gravimeter (upper dataset). Each point represents 1 minute of tide corrected gravity data. The continuous lines are running averages (30 minutes). The histograms show distribution of the 1 minute data points around the mean (for every 30 minute interval). Compared to the classical instrument, the measurement noise of the atom interferometer is smaller by a factor of 3 for equivalent measurement times. The noise per drop (launch), on the other hand, is comparable. Both instruments obvserve a slight increase in $g$ over the measurement time period due to changes in atmospheric pressure. The difference in the absolute gravity value is mostly due to the different measurement height of the two instruments (see text).

| | | | |
|---|---|---|---|
| Atom interferometer gravity value | | 979,933,160 | ± 3 |
| Falling corner-cube gravity value | − | 979,933,300 | ± 2 |
| Measurement height correction | + | 147 | ± 5 |
| Difference | | 7 | ± 7 |

Table 3: Comparison between atom interferometer and falling corner-cube gravity measurements. An independent measurement of the gravity gradient (using LaCoste-Romberg spring-type gravimeters) is used to compensate for the $\sim 0.5$ m of difference in measurement height. The atom interferometer gravity value is slightly higher.

To compare the absolute gravity values one first has to apply a gravity gradient correction to compensate for the $\sim 0.5$ m difference in the measurement height of the two instruments. However, even after applying this correction and we first found an offset of 175 $\mu$Gal. Using a new value for the cesium $D_2$ transition frequency[b], which differs by 50 MHz from the previously used value of Avila *et.al.*,[26] reduced the discrepancy to approximately 40 $\mu$Gal.

Most of the remaining 40 $\mu$Gal discrepancy was later traced to an Coriolis effect and to a disturbance of the vibration isolation system by magnetic fields. Figure 7 shows a graphical representation of the systematic effects that we have considered and analyzed in this context. A more detailed discussion of these effects, in addition to an extensive analysis of the noise sources limiting the measurement resolution, can be found elsewhere.[16,27]

After the known systematic shifts were eliminated, we performed another 2 day measurement of $g$ and found a difference of $7 \pm 7$ parts per billion with respect to the earlier FG-5 value (See Table 3). The combined uncertainty of this comparison is dominated by the uncertainty in the measurement of the local gravity gradient.

[b]This value was measured using a phase coherent frequency chain by Hänsch *et.al.* at the Max-Planck-Institute for Quantum Optics

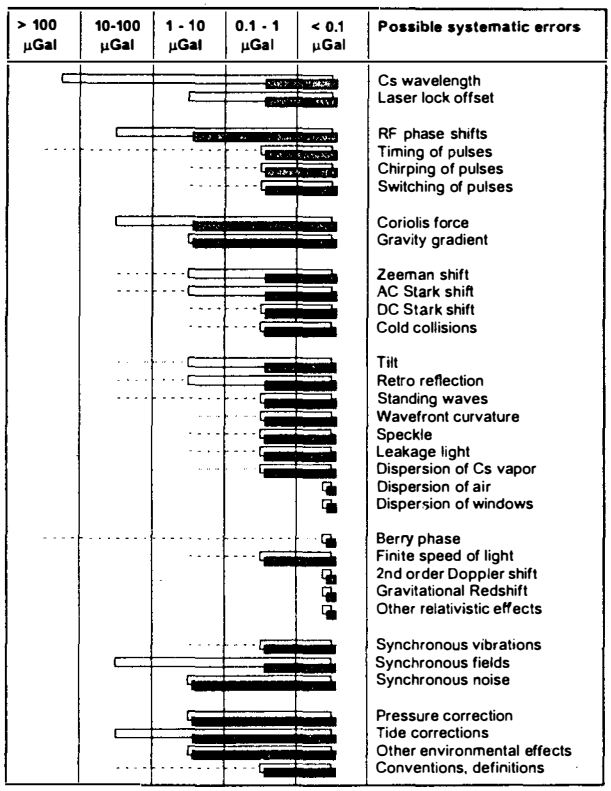


Figure 7: Summary of systematic errors. Hollow bars indicate the original size of the effect before experimental improvements, solid bars the current size. Dotted lines indicate the potential size of the effect for different experimental configurations.

## 4 Summary and Outlook

We have demonstrated an atom interferometer that can measure $g$ with a resolution of $\Delta g/g = 2 \times 10^{-8}$ after a single 1.3 s measurement cycle and $1 \times 10^{-10}$ after 2 days of integration time. The estimated accuracy of the instrument is 3 parts in $10^9$, which is by far the highest accuracy achieved by any matter wave interferometer up to now. Furthermore, from our study of the systematic effects of this measurement, we feel that straight forward improvements, particularly better zeroing of the Coriolis force, should lead to an accuracy on the order of one part in $10^{10}$.

Future experiments could use the techniques developed here to perform tests of the equivalence principle or to measure Newton's gravitational constant, $G$. In particular, the method seems well suited to measure gravitational forces at the sub-centimeter scale and to search for new short-range interactions that have been predicted by various theories.[28,29]

### Acknowledgments

We wish to thank G. Sasagawa, H. G. Scherneck, J. Goodkind, M. McWilliams and R. Jachens for helping in the geophysical aspects of this work. K.Y.C. was supported by the National University of Singapore. This work is supported in parts by the NSF and the AFOSR.

**References**


1. O. Carnal and J. Mlynek, Phys. Rev. Lett. **66**, 2689 (1991).
2. D. W. Keith, C. R. Ekstrom, Q. A. Turchette, and D. E. Pritchard. Phys. Rev. Lett. **66**, 2693 (1991).
3. F. Riehle *et al.*, Phys. Rev. Lett. **67**, 177 (1991).
4. M. Kasevich and S. Chu, Appl. Phys. B **54**, 321 (1992).
5. I. Marson and J. E. Faller, J. Phys. E **19**, 22 (1988).
6. W. A. Prothero and J. M. Goodkind, J. Sci. Instrum. **39**, 1257 (1968).
7. J. M. Goodkind, in *Near zero*, edited by J. D. Fairbank (W.H. Freeman, New York, 1988), pp. 784–794.
8. G. P. Arnautov *et al.*, Metrol. **19**, 49 (1983).
9. T. M. Niebauer, G. Sasagawa, J. Faller, and R. Hilt, Metrol. **32**, 159 (1995).
10. A. Peters *et al.*, Philos. Trans. R. Soc. London, Ser. A **355**, 2223 (1997).
11. B. Young, Ph.D. thesis, Stanford University, 1997.
12. T. L. Gustavson, P. Bouyer, and M. Kasevich, Phys. Rev. Lett. **78**, 2046 (1997).
13. D. S. Weiss, B. C. Young, and S. Chu, Appl. Phys. B **59**, 217 (1994).
14. K. Moler, D. S. Weiss, M. Kasevich, and S. Chu, Phys. Rev. A **45**, 342 (1992).
15. R. P. Feynman and A. R. Hibbs, *Quantum Mechanics and Path Integrals* (McGraw-Hill, New York, 1965).
16. A. Peters, Ph.D. thesis, Stanford University, 1998.
17. E. L. Raab *et al.*, Phys. Rev. Lett. **59**, 2631 (1987).
18. K. E. Gibble, S. Kasapi, and S. Chu, Opt. Lett. **17**, 526 (1992).
19. D. S. Weiss *et al.*, in *Light Induced Kinetic Effects on Atoms, Ions and Molecules*, edited by I. Moi *et al.* (ETS Editrice, Pisa, 1991), pp. 35–44.
20. A. Kastberg *et al.*, Phys. Rev. Lett. **74**, 1542 (1995).
21. J. M. Hensley, A. Peters, and S. Chu, J. Sci. Instrum. (to be published).
22. C. Shum *et al.*, J. Geophys. Res. **102**, 25173 (1997).
23. D. McCarthy, IERS technical note 21, U.S. Naval Observatory (unpublished).
24. H. G. Scherneck, Geophys. J. Int. **106**, 677 (1991).
25. C. Le Provost *et al.*, J. Geophys. Res. **99**, 24777 (1994).
26. G. Avila, P. Gain, E. de Clercq, and P. Cerez, Metrol. **22**, 111 (1986).
27. A. Peters, K. Y. Chung, and S. Chu, Nature (to be published).
28. S. Dimopoulos and G. Giudice, Phys. Lett. B **379**, 105 (1996).
29. J. Long, H. Chan, and J. Price, Nucl. Phys. B **539**, 23 (1999).